Welding in the World
https://doi.org/10.1007/s40194-025-02043-0

RESEARCH PAPER

Fatigue behaviour of 12-month corroded offshore steel joints under accelerated salt spray exposure: an experimental and numerical analysis

Sulaiman Shojai[1,2] · Kram Kabha[2] · Christian Woitzik[3] · Moritz Braun[1] · Elyas Ghafoori[2]

Received: 23 July 2024 / Accepted: 6 April 2025

Abstract
The fatigue strength of steel structures can decrease significantly when corrosion occurs. Pitting corrosion, in particular, can lead to locally high stress concentrations and may interact with existing stress concentrations from weld seams. Particularly in the case of offshore support structures, which are exposed to a corrosive environment and include several welded connections, this issue becomes relevant. Hence, in this study, butt- and fillet-welded joints of structural steel were exposed to accelerated corrosion in a salt spray chamber and then tested for fatigue strength. In order to investigate the long-term behaviour, the specimens were stored for 12 months in a salt spray chamber. Base material specimens were investigated as reference. All specimens were clean blasted and 3D scanned prior to the fatigue tests. It was shown for all specimens that the fatigue strength decreased after 12 months compared to the uncorroded reference tests. However, the fatigue reduction was different for the different geometries. The greatest reduction was observed for the base material from 282 to 122 N/mm^2, followed by butt-welded joints from 215 to 147 N/mm^2, and fillet-welded joints from 168 to 144 N/mm^2. As the fatigue strengths showed only minor difference after 12 months, an equalization effect can be assumed. The results show that a generalized reduction of the fatigue strength, in accordance with the guidelines, is not appropriate and therefore should be revised for a more accurate design of offshore support structures. Finally, numerical analysis based on 3D scans of the specimens was conducted and compared with the test results.

Keywords Weld seams · Pitting corrosion · Stress concentrations · Long-term corrosion · Corrosion fatigue · 3D digital scans · Digital twins

Symbols

K_t	Notch stress concentration factor
K_f	Effective notch stress concentration factor
$K_{f,crack}$	Effective notch stress concentration at the crack location
$K_{f,max}$	Effective maximum notch stress concentration
ΔK_{th}	Fatigue crack propagation threshold
$\Delta\sigma_c$	Characteristic fatigue strength
$\Delta\sigma_{c,10\%}$	Characteristic fatigue strength for 10% survival probability
$\Delta\sigma_{c,90\%}$	Characteristic fatigue strength for 90% survival probability
$\Delta\sigma_f$	Effective notch stress range
$\Delta\sigma_n$	Nominal stress range
$\Delta\sigma_0$	Fatigue limit
$\dot{q}$	Heat flux boundary condition
ρ_d	Density
$\sigma_f(x)$	Effective notch stress function
σ_k	Notch stress
σ_n	Nominal stress
c_p	Specific heat capacity
T_σ	Scatter coefficient
λ	Thermal conductivity parameter
a	Weighting parameter

Recommended for publication by Commission XIII - Fatigue of Welded Components and Structures

✉ Sulaiman Shojai
sulaiman.shojai@dlr.de

Elyas Ghafoori
ghafoori@stahl.uni-hannover.de

[1] German Aerospace Center (DLR), Institute of Maritime Energy Systems, Geesthacht, Germany

[2] Institute for Steel Construction ForWind, Leibniz University Hannover, Hanover, Germany

[3] Institute for Ship Structural Design and Analysis, Hamburg University of Technology, Hamburg, Germany

Published online: 14 June 2025

m	Slope of S–N curve
$\dot{q}$	Heat flux boundary condition
G	Weighting function
L	Intrinsic material length
N	Number of cycles to failure
V_r	Reference volume

Abbreviations

DIC	Digital image correlation
DNV	Det Norske Veritas
ERF	Environment reduction factor
GMAW	Gas metal arc welding
HAZ	Heat-affected zone
IGM	Implicit gradient model
SAW	Submerged arc welding
SED	Strain energy density
S-N	Stress-life (curve)
SSC	Salt spray chamber
TCD	Theory of critical distances

1 Introduction

Offshore support structures face harsh environmental conditions and fatigue loads. These conditions limit the service life of the corrosion protection systems and the support structures. When the corrosion protection system degrades or becomes damaged, corrosion occurs. Especially in the case of unplanned damages from mechanical impacts, which can happen much earlier than the complete degradation of the protection, the steel is exposed to free corrosion for a long period. Pitting corrosion, in particular, leads to notch effects due to significant local stress concentrations. These stress concentrations can reduce the fatigue strength of the support structures and their (remaining) service life. The impact of pitting corrosion on the fatigue strength of steel plates has been extensively studied [1–4]. However, in practical applications, steel structures comprise numerous welded joints, which are typically the most critical areas due to the high local stress concentrations. Thus, for the evaluation of the remaining service life, the interaction of notch stress concentration of pitting corrosion and welds and its impact on fatigue becomes important. A general distinction can be made between corrosion fatigue (CF) and the fatigue of pre-corroded metals. CF occurs under simultaneous exposure to corrosion and fatigue, while in the case of pre-corroded metals, corrosion occurs first, followed by fatigue in air. Physically, the two phenomena differ in that CF involves both anodic dissolution and material embrittlement. In contrast, with preceding corrosion, embrittlement also occurs but is localized to the surface and does not affect crack propagation during the subsequent fatigue test in air.

The CF test is commonly performed in artificial seawater, where the exposure duration is limited to approximately 1 month due to the chosen test frequency of 0.2–0.5 Hz. While this frequency matches the first eigenfrequency of offshore support structures, it results in less pitting corrosion development compared to offshore support structures that corrode freely over many years and thus do not represent the long-term behaviour of the steel surface. Therefore, specimens are often pre-corroded in a salt spray chamber (SSC) to accelerate the process. Usually, the specimens are exposed in the SSC for up to 1 month [5, 6] or in some cases up to 3 months [7], and then fatigue tested in air. Although this approach does not cover the CF behaviour, it provides the opportunity to investigate the notch effect resulting from pitting corrosion typically observed after long-term corrosive exposure. However, it cannot be assumed that an exposure period of 1–3 months is equivalent to the long-term exposure of several years that offshore support structures might experience. To determine this, fatigue tests with varying corrosion durations would need to be conducted to identify a potential saturation behaviour after a certain period, which has not yet been investigated.

In Addition to that, current regulations such as DNV [8] and also IIW [9] do not distinguish between different specimen geometries (notch classes) when it comes to fatigue life reduction due to corrosion. In DNV [8], all existing stress-life (S–N) curves are reduced by a constant environment reduction factor (ERF) of ERF = 3 in order to consider a free corrosion situation. According to the IIW standard [9], it is recommended to reduce the S–N curves by at least 30% without any further specification. The approach of constant reduction is very questionable, as ERF of highly notched components, such as tubular joints, indicate lower values than moderately notched components, such as butt welds [10]. This could also be observed by Yuasa and Watanabe [11], who tested pre-corroded fillet and butt welds, finding that the fatigue strength of the butt-welded joints decreased, while it remained unchanged for the fillet-welded joints. They suggested that the already sharp notches in the fillet welds could not be further intensified by corrosion, whereas the stress concentration in the butt welds had greater potential to increase due to their initially lower notch sharpness.

To include potential differences arising from different specimen geometries, base material, butt-welded, and fillet-welded specimens were investigated in this study. The specimens were clean blasted in accordance with real offshore support structures. In order to close the knowledge gap regarding the long-term behaviour, the specimens were pre-corroded in a SSC for 12 months. Subsequently, fatigue tests were conducted and compared with results of uncorroded and 1-month corroded specimens in order to show the development over time

and observe a potential saturation phenomenon. Additionally, the specimens were scanned using 3D scanners in order to analyse the notch stress concentrations based on the real surface geometry.

The novelties of this study can be summarized as follows:

- Fatigue tests on base material, butt-welded, and fillet-welded specimens, after clean blasting and long-term pre-corrosion (12 months) in a salt spray chamber
- Numerical analysis of stress concentrations based on 3D scans, including pitting corrosion and weld geometry
- Consideration of the micro-support effect with the implicit gradient model (IGM)
- Comparison of fatigue test results with numerically predicted crack locations

The results can contribute to the understanding of fatigue behaviour of long-term corroded steel structures and the analysis of the (remaining) service life based on 3D surface scans.

2 Materials and methods

2.1 Experimental analysis

2.1.1 Specimen fabrication preparation

In the framework of this study, both base material specimens (*G*) and welded specimens with a thickness of 12 mm made of low-alloy structural steel EN 10225 S355G10 + M (similar to ASTM A131 EH36) were investigated. The material properties are summarized in Table 1. The tested specimen geometries are shown in Fig. 1(a). In Fig. 1(b, c), the macrographs for a fillet-welded specimen are illustrated before and after the corrosion process.

For the welded specimens, double V-shaped butt welds (*S*) and fillet welds (*K*) were examined. Specimens with fillet welds included non-load-carrying transverse stiffeners, which were welded on a continuous plate with a throat thickness of 4 mm. Fillet welds were produced using the gas metal arc welding (GMAW) process with T46 6 M M 1 H5 consumables. Butt welds were produced using the

Table 1 Material properties S355G10 + M

Chemical composition (%)								
C	Si	Mn	P	S	N	Al	Cu	Cr
0.06	0.27	1.37	0.012	0.001	0.005	0.036	0.02	0.03
Mechanical properties:								
Yield stress $R_{p0.2}$ (N/mm^2)			Ultimate strength R_m (N/mm^2)			Elongation A5 (%)		
421			493			35		

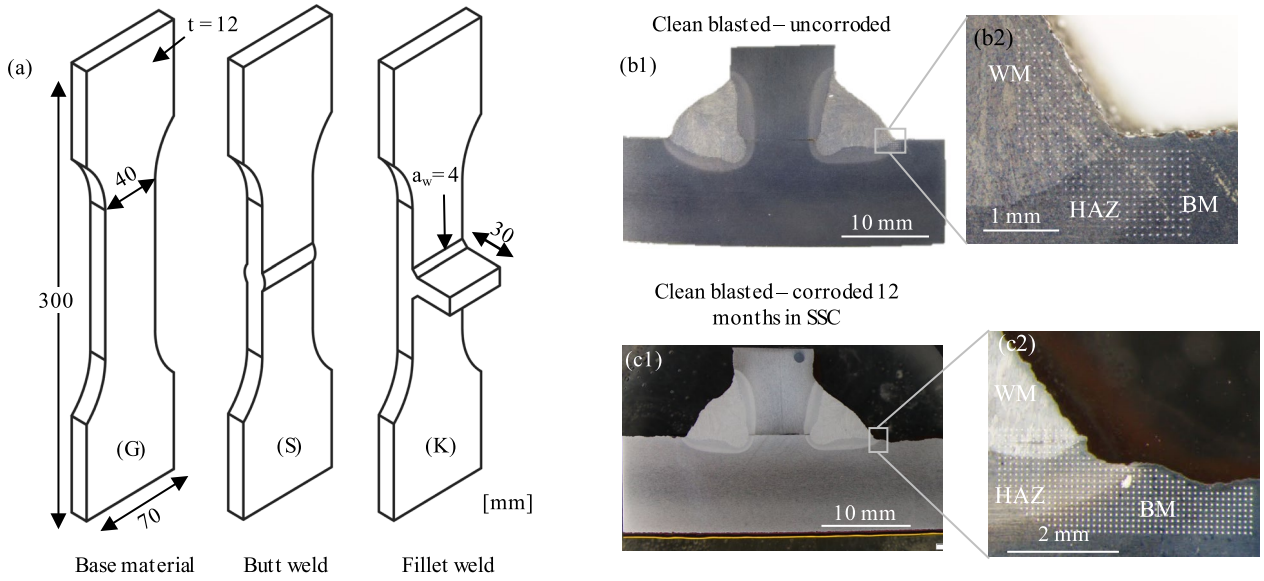

Fig. 1 **a** Specimen geometries for base material (*G*), butt weld (*S*), and fillet weld (*K*); **b**, **c** macrographs for fillet welds before and after corrosion exposure

submerged arc welding (SAW) process with S3Si consumables. In both cases, the limits for irregularities are in line with the evaluation group B according to ISO 5817 [12].

After welding, the specimens were cut into 70-mm strips from a metal sheet of 1000 mm length and 300 mm width by water jet. Then, the specimens were clean blasted according to the requirements of DNV RP- 0416 [13] for real offshore support structures, in order to clean and roughen the surface for the subsequent application of the corrosion protection. Grit was used as the blasting medium. For the investigated specimens, cleanliness grades of Sa 2 ½ to 3 according to ISO 8501–1 were achieved. In Table 2, the test matrix with the number of specimens for each test series for the three different geometries (*G*, *S*, and *K*) and the different corrosion durations (0, 1, and 12) are illustrated. Here, '0' refers to clean-blasted and uncorroded condition, while '1' refers to 1-month (1 M) and '12' to 12-month (12 M) corrosion exposure. The uncorroded and 1 M corroded specimens were already presented in [5]. The main focus of this work is on the 12-month long-term corroded specimens.

After clean blasting, corrosion protection was applied to the clamping area of the specimens, in order to ensure an even surface and a uniform loading of the specimen. In the area of the welds, no corrosion protection was applied. After the corrosion process, the specimens were cut into the typical shape shown in Fig. 1(a). Moreover, the edges were chamfered to avoid crack initiation from there.

2.1.2 Corrosion exposure

Corrosion experiment After preparation, the specimens were stored in the standardized salt spray chamber according to ISO 9227 [14] and were exposed to a 5% natrium-chloride solution. Therefore, the steel specimens were placed at an angle between 15 and 20° from the vertical so that the surfaces were fully exposed to the salt spray; see Fig. 2. In addition, it was ensured that the steel specimens did not touch the chamber walls. For the preparation of the spray medium, natrium-chloride was dissolved in distilled and deionized water. In the salt spray chamber, the spray medium is sprayed to the chamber roof for a uniform distribution on the steel specimens. The pH value of the spray medium was between 6.5 and 7.2 at (25 ± 2) °C and was continuously checked and adjusted if necessary. About 12 specimens for each geometry (see Table 2) were exposed to free corrosion in the SSC for a duration of 1 and 12 months.

Rust removal The rust on the specimens was removed according to ISO 8407–1 [15] in a hydrochloric acid bath, which is prepared in the ratio of 1000 ml hydrochloric acid (HCl), 20 g antimony trioxide (Sb_2O_3), and 50 g tin(II)chloride ($SnCl_2$). Before storing the specimens in the hydrochloric acid bath, the specimens were mechanically cleaned with a wire brush until large and loose pieces of the corrosion products were removed. The storage time in the hydrochloric acid bath was between 5 and 30 min. In Fig. 3, the specimen before and after rust removal is shown.

Table 2 Test matrix including different surface conditions and weld types

Surface condition	Specimen geometry		
	Base material (series)	Butt weld (series)	Fillet welds (series)
Clean blasted (tested in [5])	$12 \times (0 - G)$	$12 \times (0 - S)$	$12 \times (0 - K)$
Clean blasted — corroded 1 month (tested in [5])	$12 \times (1 - G)$	$12 \times (1 - S)$	$12 \times (1 - K)$
Clean blasted — corroded 12 months	$11 \times (12 - G)$	$13 \times (12 - S)$	$9 \times (12 - K)$

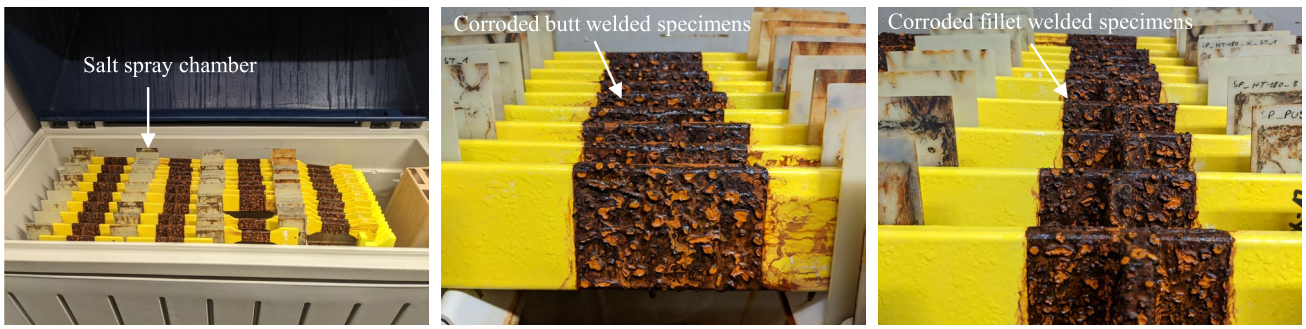

Fig. 2 Specimens stored in the salt spray chamber — condition after 1 month exposure

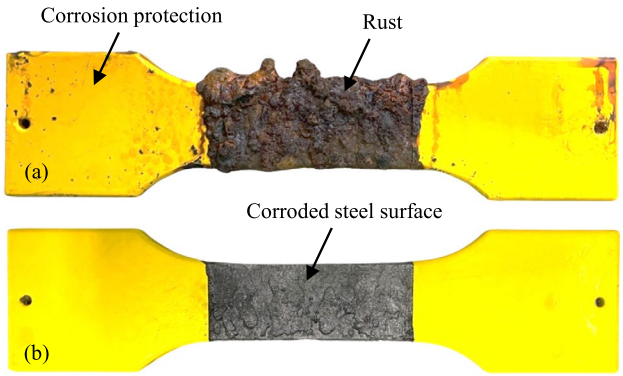

Fig. 3 Twelve-month corroded base material specimen **a** before and **b** after rust removal

2.1.3 Fatigue tests

Fatigue tests were carried out on a servo-hydraulic fatigue testing machine MFL HUS 60. The specimens were loaded axially with a frequency between 8 and 10 Hz and a mean stress ratio of $R = 0.1$ until total failure. The specimens were clamped on both sides, which introduced additional mean stresses due to misalignments of the specimens, resulting in a higher effective R-ratio. Before clamping, the corrosion protection on the clamping area was removed in order to avoid slippage of the specimens. Some fatigue tests were monitored with digital image correlation (DIC) in order to capture the crack initiation location. In other cases, the crack locations were determined by analysing the beach marks on the cracked cross section.

2.2 Numerical analysis

The numerical analysis comprises a total of four individual steps; see Fig. 4. The basis for the numerical analysis is a 3D scan of the real specimen. Therefore, in the first step, all specimens tested for fatigue were scanned using a 3D scanner and transferred to a 3D solid model via reverse engineering. The 3D solid model is used to determine the fatigue-driving (effective) notch stress concentrations. Therefore, the clamping process (step no. 2) is simulated first. The offset to the plain line resulting from angular and linear misalignment is eliminated and the specimens are straightened analogous

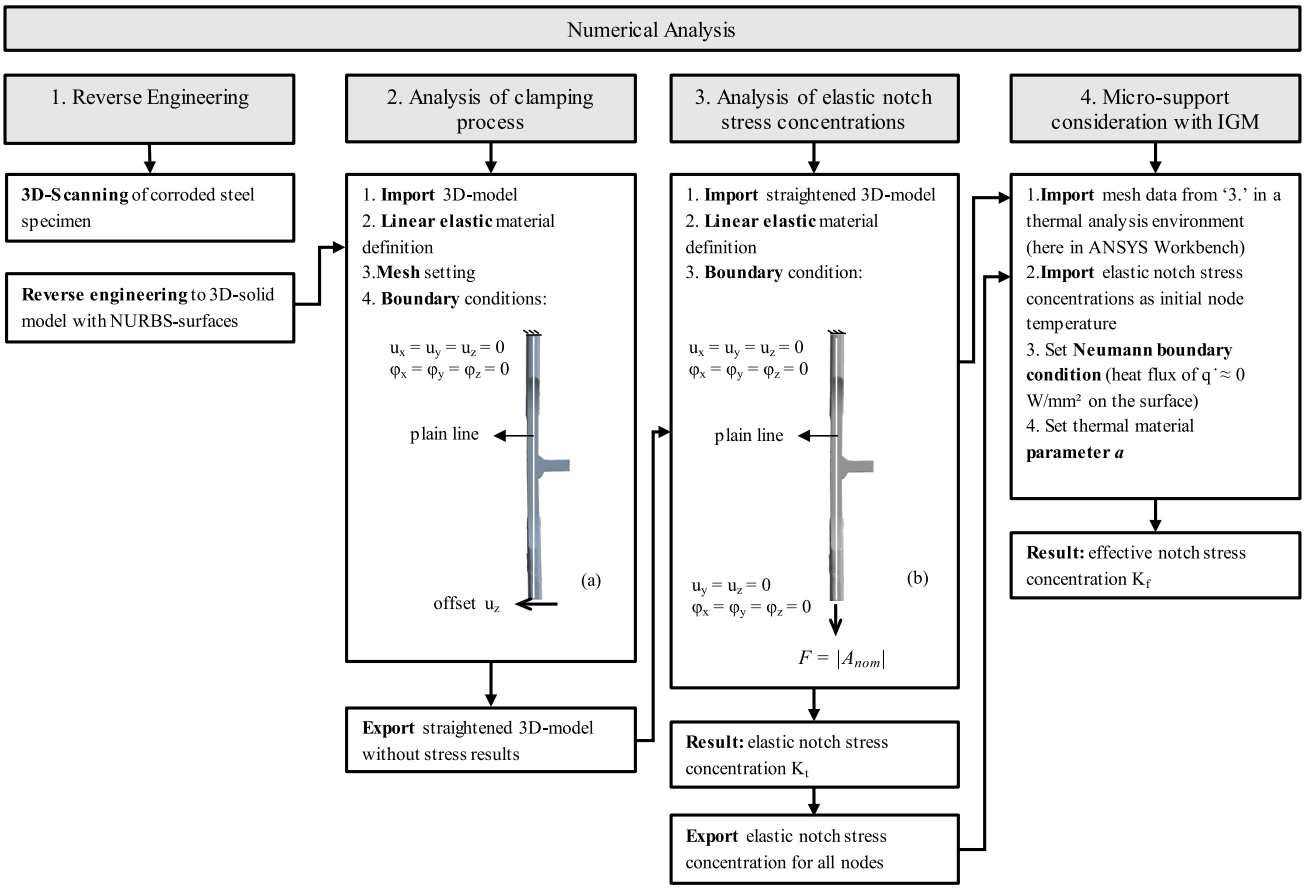

Fig. 4 Flowchart of numerical analysis using the IGM approach

to reality. The straightened specimen is then used in step 3 to determine the elastic notch stress concentrations. Finally, in step 4, the micro-support effect is taken into account on the basis of the IGM in order to derive the effective stress concentrations. The elastic notch stress concentrations are used as the basis for the calculation. The numerical investigation was limited to the welded specimens because of the high effort involved, and given that the interaction of weld notches and pitting notches is the most interesting aspect. It should be noted that throughout the paper, the term 'effective stress concentration' refers to the stresses derived by the IGM approach.

2.2.1 Reverse-engineering and numerical model

The reverse engineering process for the examined specimens in this study included several steps. The procedure started with scanning the whole specimen with the optical 3D scanner ATOS Core 300 5 M from GOM with a resolution of 0.12 mm. This ensures that global imperfections such as linear and angular misalignment are included and is hence called as 'global scan'. In order to ensure a high accuracy at the weld seams, additional measurements were performed using the 3D profilometer Keyence VR- 3000 with a resolution of 0.02 mm, also called 'local scan'. In Fig. 5, a corroded fillet-welded specimen and the corresponding global and local scans are shown. It becomes obvious that the local scan includes more detail about the surface than the global scan. For the numerical model, the welded area of the global scan is replaced with the high-resolution scan of the profilometer and then converted to a 3D solid model, as shown in Fig. 6 for all specimen geometries. More details on the reverse engineering process can be found in [2, 16, 17]. For the discretization, quadratic tetrahedral elements were used, as shown in Fig. 7(b). In the welded area, the element lengths are set to $l_e = 0.1$ mm, while at other corroded areas, they are set to $l_e = 0.4$ mm. In the clamping area, where no corrosion occurred because of the corrosion protection, the

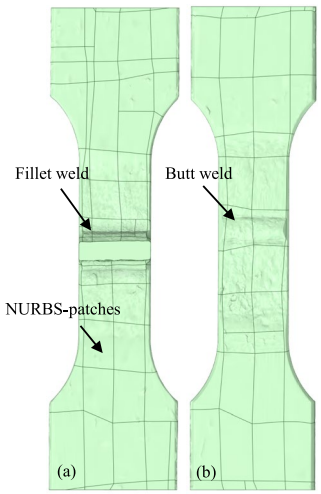

Fig. 6 3D solid models for (**a**) butt- and (**b**) fillet-welded specimens built from NURBS patches

element size was set to $l_e = 1.0$ mm. In previous research [2, 16, 17], the element size was set based on a convergence study of the elastic notch stress concentrations, which led to smaller element lengths of $l_e = 0.02$–0.05 mm. In this analysis, the element length was set based on a convergence study of the effective notch stress concentration. In Fig. 7(c), the result of the convergence study is illustrated. For element lengths greater than or equal to $l_e = 0.1$ mm, the relative change tends to be zero. Hence, in the welded area, the element length was set to $l_e = 0.1$ mm.

2.2.2 Simulation of clamping process

As already mentioned, the specimen included linear and angular misalignment after the fabrication. In the clamping process, where one side of the specimen (here the upper side) is clamped first, the misalignments lead to an offset between the ends of the specimen. While the existing offset between the ends is eliminated by clamping the lower side, it

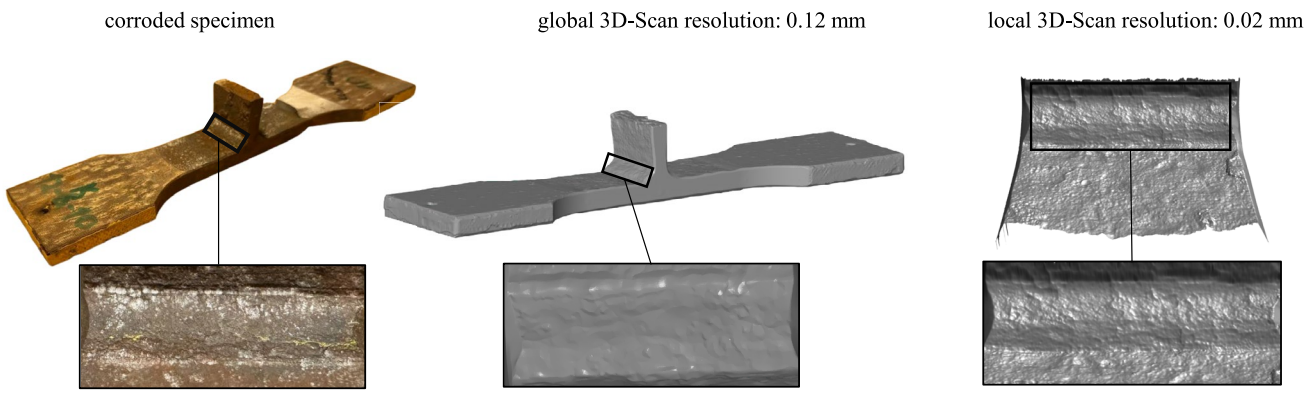

Fig. 5 Scanning of the specimen in different resolutions

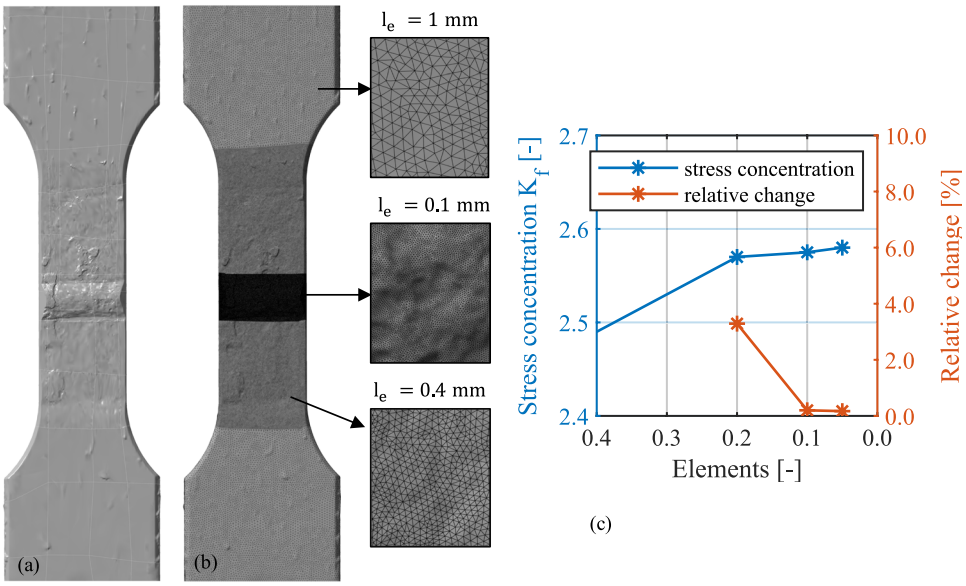

Fig. 7 (**a**) 3D-numerical model and (**b**) discretization of the model (**c**) convergence analysis

leads to additional bending stresses. However, in this study, the simulation of the clamping process is only used to eliminate the offset. This ensures that the subsequently determined stress concentrations include only the influence of the axial load applied to the specimen during the experiment.

For the numerical simulation, the model and the mesh from Fig. 7 were used. The material was considered as linear elastic. The boundary conditions are applied according to Fig. 4(a). The offset is calculated for each specimen separately with a MATLAB tool based on the scanned data of the whole specimen and is applied as a displacement in the z-direction. From the comparison of the plain line illustrated in Fig. 4(b), it becomes evident that the offset is eliminated after the application of the deformation.

2.2.3 Analysis of elastic notch stress concentration

Similar to the simulation of the clamping stresses, the stress concentrations are calculated based on linear elastic material formulation. Analogous to the fatigue test, the model is fixed on both sides, allowing only axial deformation; see Fig. 4(b). The applied force equals the magnitude of the cross section in the tailed area with $F = |A_{\mathrm{nom}}| = 480$ N, which leads to a nominal stress $\sigma_{\mathrm{n}} = 1$ N/mm^2 and allows the resulting notch stresses to be interpreted as notch stress concentration factors ($\sigma_{\mathrm{k}} = K_{\mathrm{t}}$). It should be noted that for all specimens, the initial cross section before clean blasting and corrosion was considered.

2.2.4 Consideration of micro-support effect

The micro-support effect is related to the behaviour of micro cracks during cyclic loading. Particularly, in the case of sharp notches, the yield stress in the surface crystallites can be exceeded and lead to micro cracks, which may not propagate with continued cyclic loading. This behaviour reduces the local stresses and supports the fatigue resistance [18, 19]. The reduced local stresses are referred to as effective notch stresses. Various micro-support effect hypotheses can be found in the literature for calculating the effective notch stress, such as the strain energy density (SED) method [20–22]; the theory of critical distances (TCD) [23–25], see Fig. 8(a) and (b); or the implicit gradient model (IGM) [26–28], see Fig. 8(c). The main idea of all theories is that the fatigue-driving stress (or strain) is not the stress at the surface of a component, but rather a stress at a certain depth or a stress averaged over a certain length, area, or volume.

The TCD method is primarily applied in cases where the number of notches and potential crack locations is limited, such as in a welded structure analysed using a 2D FE model. When dealing with a high number of individual notches, as it is the case with 3D models based on scans, the post-processing effort becomes highly demanding. This effort is further increased for corroded specimens, where a large number of pits exist, each of which can be critical for crack initiation. To avoid the extensive post-processing required for every single notch, in this study, the micro-support effect was considered by the IGM approach. The IGM approach allows the micro-support effect to be taken into account within the numerical analysis of the stress field. This enables the consideration of all existing notches of a corroded component in a single numerical analysis. According to IGM, the effective notch stress $\sigma_{\mathrm{f}}(\boldsymbol{x})$ at the point $\mathbf{x} = (x_1, x_2, x_3)$ can be described as the integral over the volume V of the weighting function G, which is dependent on the distance $\|x - y\|$ between point

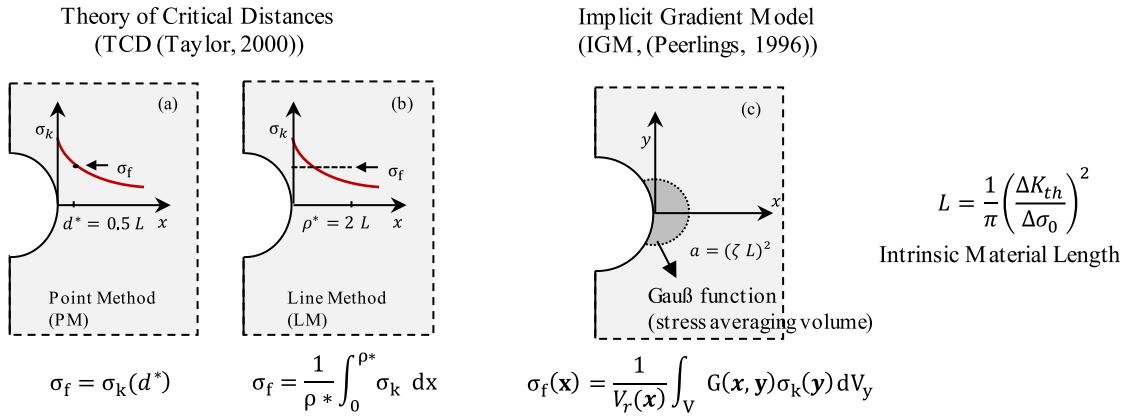

Fig. 8 Micro-support consideration with **a**, **b** the theory of critical distances and **c** the implicit gradient model

x and any point $y = (y_1,y_2,y_3)$, and a reference volume V_r as follows:

$$\sigma_f(x) = \frac{1}{V_r(x)}\int_V G(x,y)\sigma_k(y)dV_y \tag{1}$$

Assuming a Gaussian function for the weighting function $G(x,y)$, that approximates the hemisphere in Fig. 8 (c), this leads to the following differential equation:

$$\sigma_f(\vec{x}) - \sigma_k(\vec{x}) - a\nabla^2\sigma_f(\vec{x}) = 0 \tag{2}$$

where the parameter a (> 0) corresponds to the weighting factor of the surrounding volume at the notch and is linked to the intrinsic material length L with:

$$a = (\zeta \times L)^2 \tag{3}$$

where ζ considers the stress criterion, which is equal to 0.545 for the maximum principal stress, as well as for the Tresca stress criterion, and 0.456 for the von Mises stress criterion [29].

The total volume of the body is considered as the solution domain, and the surface is defined as the boundary. Usually the Neumann boundary condition is used [26, 30]:

$$\frac{\partial\sigma_f(x)}{\partial x} \times n = 0 \tag{4}$$

where n is the normal to the surface of the solution domain.

For consideration of the micro-support effect with IGM, the differential Eq. (2) has to be solved for σ_f for any given stress σ_k. For one- or two-dimensional problems, the equation can be solved by numerical computation. For three-dimensional problems, it is recommended to use the solvers of commercial FE software. According to Lang et al. [31] and Lener et al. [32], it can be solved with the thermal analysis module of commercial FE software, as Eq. (2) can be transformed into the differential equation of the thermal diffusion problem. For more information on the numerical implementation, it is referred to Shojai et al. [33].

In this study, the thermal analysis module of ANSYS Workbench is used to solve Eq. (2). For this purpose, the elastic notch stresses σ_k ($= K_t$) are used as input values for the diffusion analysis for each individual node of the numerical model from Fig. 7. The Neumann boundary condition according Eq. (4) is considered with a 'heat flux' boundary condition of $\dot{q} \approx 0$ applied to the surface of the specimen. The weighting parameter a is linked to the thermal properties with $a = \frac{\lambda}{\rho_d \times c_p}$ and is considered with the thermal conductivity parameter λ, as the specific heat capacity and density were set to $c_p = 1.0$ and $\rho_d = 1.0$. Based on literature review, the parameter can be set to $a = 0.01$ mm^2 for mild structural steel. For more details, the following literature is recommended: [16, 28, 33, 34] Table 3.

Table 3 Parameter of S–N curves

Geometry	Corrosion exposure duration	Slope m	Fatigue strength $\Delta\sigma_c$ (N/mm^2)	Scatter T_σ
Base material	Uncorroded	− 14.8	282	1.09
	1 M	− 14.5	251	1.17
	12 M	− 4.9	122	1.22
Butt welds	Uncorroded	− 9.4	215	1.28
	1 M	− 6.6	160	1.42
	12 M	− 6.9	147	1.13
Fillet welds	Uncorroded	− 6.7	168	1.29
	1 M	− 3.8	109	1.43
	12 M	− 5.5	144	1.13

3 Results

3.1 Results of fatigue tests

The tests were evaluated in accordance with Eurocode 3 [35] using linear regression according to the least squares method in the direction of the number of cycles. Additional stress magnification factors caused by misalignments of individual specimens were not considered here. Run-outs were not taken into account in the evaluation and are also not shown in the diagrams. Instead, the run-out specimens were retested at a new load level if no cracks could be detected. In Table 4, all fatigue test results for the 12 M corroded specimens, including the run-outs, are summarized. For all test series, the corresponding S–N curves, defined as

$$N = 2 \times 10^6 \times \left(\frac{\Delta\sigma_c}{\Delta\sigma_n} \right)^m \tag{5}$$

were derived. In the equation, N represents the number of cycles to failure, $\Delta\sigma_n$ is the variable nominal stress range, m is the slope, and $\Delta\sigma_c$ is the characteristic stress range at $N = 2 \times 10^6$ cycles. Furthermore, the scatter coefficient T_σ was evaluated. This is defined as

$$T_\sigma = \frac{\Delta\sigma_{c,10\%}}{\Delta\sigma_{c,90\%}} \tag{6}$$

where $\Delta\sigma_{c,10\%}$ and $\Delta\sigma_{c,90\%}$ are the characteristic fatigue strengths derived from the S–N curve for 10% and 90% survival probability at $N = 2 \times 10^6$ cycles.

In Fig. 9 and Table 3, the resulting S–N curves and the corresponding parameters for the descriptions are given for each test series. Figure 9(a1) to (a3) show the fatigue results for all specimen geometries in S–N diagrams. The fatigue strength of the base material specimens after 12 months of corrosion exposure is $\Delta\sigma_c = 122$ N/mm^2 and is lower than that of the butt and fillet weld specimens, with $\Delta\sigma_c = 147$ N/mm^2 and $\Delta\sigma_c = 144$ N/mm^2. At the same time, the scatter in the base material specimens with $T_\sigma = 1.22$ is greater than in the butt and fillet weld specimens, with $T_\sigma = 1.13$.

The comparison of the base material specimens in the uncorroded, 1 M, and 12 M corroded conditions in Fig. 9(b1) shows that corrosion has a greater negative influence on the fatigue strength after 12 months than after just 1 month. The fatigue strength decreases over time, while the scatter increases.

Figure 9(b2) shows that the fatigue strength of the butt weld specimens also decreases between 1 and 12 M. However, the decrease is much smaller than that between uncorroded and 1 M specimens. At the same time, the initially large scatter, see Table 3, decreases over time due to the corrosion process.

In contrast to the base material and butt weld specimens, no steady decrease in fatigue strength can be observed in the fillet weld specimens; see Fig. 9(b3). Although the fatigue strength decreases from $\Delta\sigma_c = 168$ N/mm^2 to $\Delta\sigma_c = 109$ N/mm^2 after 1 month of corrosion, it increases again significantly to $\Delta\sigma_c = 144$ N/mm^2 after 12 months of corrosion, contrary to expectations. A closer examination of the individual values reveals that the majority of the tests actually show higher fatigue strength after 1 month compared to after 12 months. However, due to two individual values with relatively low fatigue strength, there is greater scatter, resulting in comparatively lower overall fatigue strength.

In Fig. 10(a), the characteristic fatigue strengths for all specimen geometries are summarized as a function of exposure duration. The different behaviour depending on the specimen geometry is evident here. In addition, it can be observed that the different specimen geometries have similar fatigue strengths after 12 months. Therefore, in Fig. 10(b), a joint evaluation of the fatigue tests on 12-month corroded specimens was carried out. The joint evaluation results in a fatigue strength of $\Delta\sigma_c = 133$ N/mm^2 and a relatively narrow scatter of $T_\sigma = 1.17$. It reveals that the slight differences in the individual evaluation are within the scatter range of the fatigue tests. The value determined for the fatigue strength is in line with previous investigations from Shojai et al. [2], where a fatigue strength of $\Delta\sigma_c = 139$ N/mm^2 was determined for pre-corroded (approx. 10–15 years as part of a dismantled ballast tank) base material specimens tested on the same mean stress ratio of $R = 0.1$ as in this study.

From the observations, it can be concluded that the notch effect from corrosion depends on the initial notch condition. The notch effect from corrosion is greater for weakly or not pre-notched components than for strongly pre-notched components such as fillet welds. Moreover, the results indicate that there is an equalization effect for long corrosion exposure durations. Regardless of the initial state, the fatigue strengths after 12 months of corrosion exposure are very similar for all specimen geometries. This is because corrosion causes weak notches to become sharper and sharp notches to become softer. In [36], the weld geometry of butt and fillet welds was evaluated based on 3D scan for different exposure durations. It revealed for butt welds that corrosion leads to a reduction of the weld toe radius and an increase of the weld toe angle, which both increase the stress concentrations. For fillet welds, it could be shown that the weld toe radius is increasing and the weld toe angle is decreasing over time, which results in lower stress concentrations compared to the uncorroded state. However, the equalization effect affects not only the fatigue strength itself, but also the scatter in the S–N curve. In the case of the unnotched base material specimens, the low initial scatter due to corrosion became larger, while the high initial scatter in the weld seam specimens became smaller.

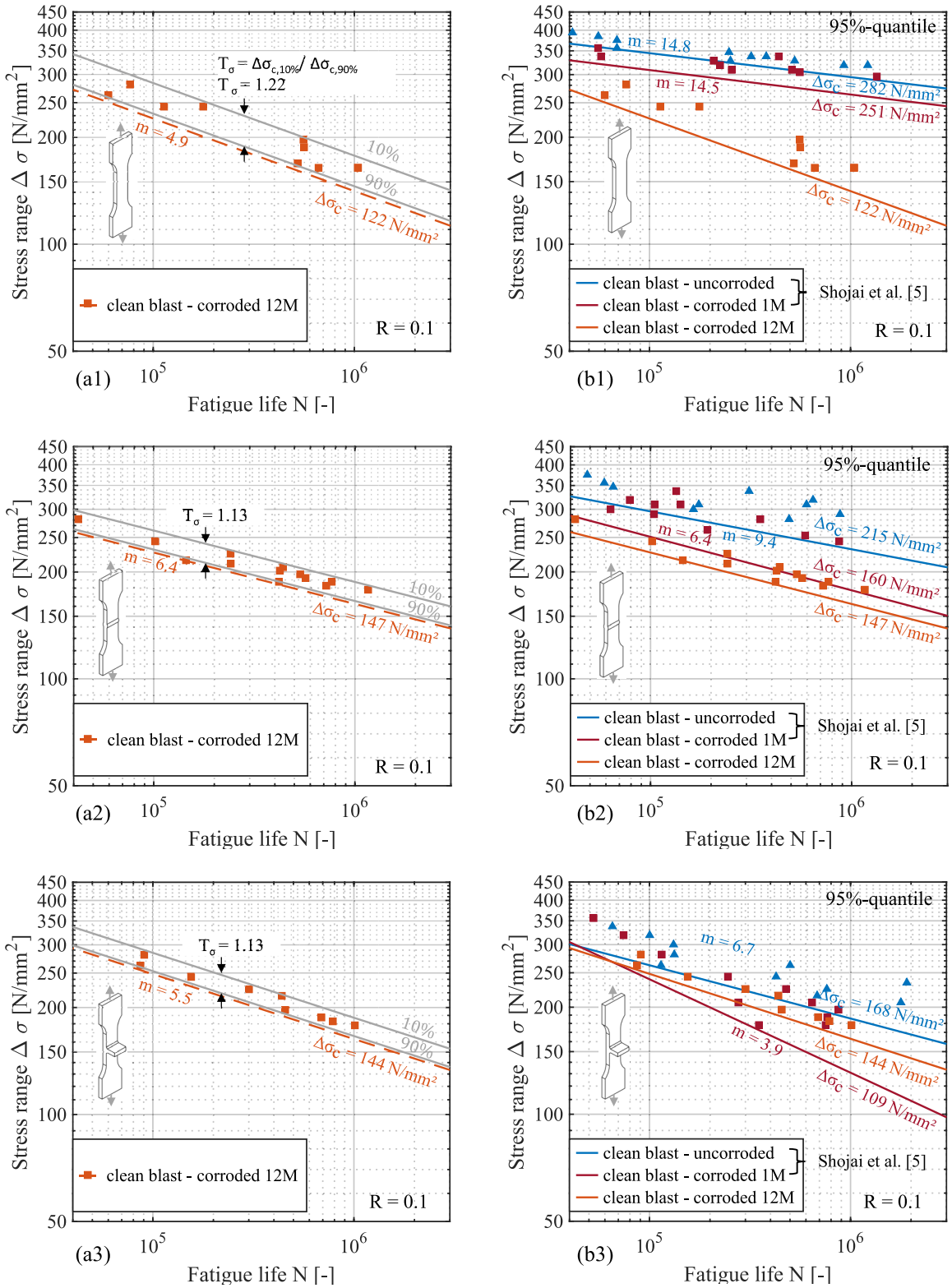

Fig. 9 Results of the fatigue tests: (a1) to (a3) results of the 12 M specimens and (b1) to (b3) results of the 12 M specimens compared to the uncorroded and 1 M specimens from [5]

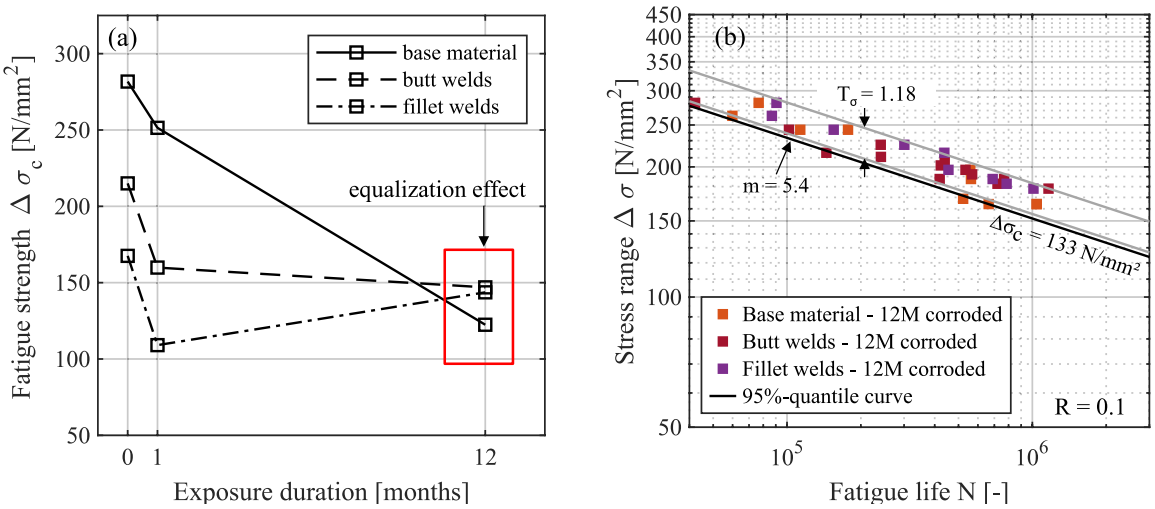

Fig. 10 A Characteristic fatigue strengths $\Delta\sigma_c$ for all specimen geometries over exposure duration and **b** joint evaluation of the fatigue tests of all specimen geometries after 12 months of corrosion exposure

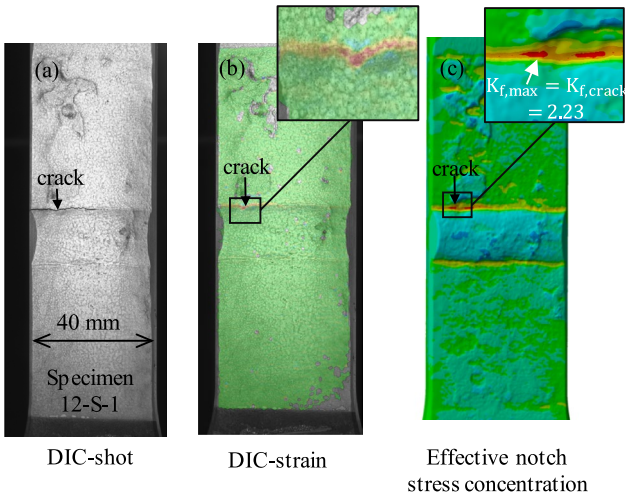

Fig. 11 Comparison of crack location captured with DIC (**a**, **b**) and effective notch stress concentration based on IGM (**c**) for 12-month corroded butt-welded specimen

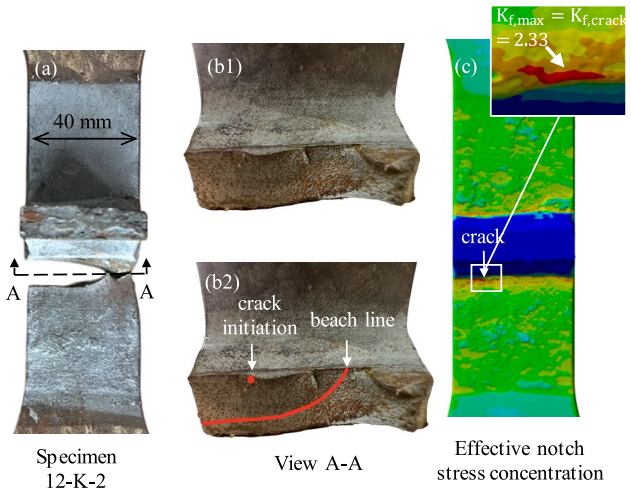

Fig. 12 Comparison of crack location based on beach line evaluation (**a**, **b**) and effective notch stress concentration based on IGM (**c**) for 12-month corroded fillet-welded specimen

3.2 Results of numerical analysis

The results of the numerical analysis are the effective notch stress concentrations K_f, which were calculated based on IGM; see Fig. 4. In Figs. 11 and 12, the effective notch stress concentrations for butt- and fillet-welded specimens are depicted. The hotspots of the effective notch stress concentrations are compared with the crack locations from the fatigue test. The crack locations from the fatigue test were tracked in the butt welds using DIC. For this purpose, images were taken at the load peak at intervals of approx. 500 to 1000 load cycles, and the strains were then evaluated; see Fig. 11(b). For the fillet-welded specimens, the crack locations were determined using the beach lines. It was assumed that the crack initiation spot is the point where the beach line has its lowest point; see Fig. 12(b).

The comparison between the actual crack location and the numerical prediction for the butt-welded specimen in Fig. 11 shows an exact match. The crack occurred at the same location where the highest effective stress concentration was predicted. A similar pattern can be observed in Fig. 12 for the fillet-welded specimen. Again, the crack occurred at the location of the highest effective notch stress concentration.

However, the presented match is not found for every specimen. The evaluations for all other specimens are shown individually in Appendix 2. It can be observed that only two of seven evaluated butt-welded specimens had an exact match, namely specimens 12-S- 1 and 12-S- 9. For fillet welds, the match is given for three of six examined specimens, namely specimens 12-K- 2, 12-K- 5, and 12-K- 11. In the evaluation, the maximum effective notch stress concentration is denoted as $K_{f,max}$ and the effective notch stress concentration at the crack location is denoted as $K_{f,crack}$. In cases where the locations match, $K_{f,max}$ equals $K_{f,crack}$. Figure 13 shows the effective notch stress concentrations $K_{f,max}$ and $K_{f,crack}$ for all tested specimens. In general, it can be observed that the effective notch stress concentrations for butt welds are lower than for fillet welds. For specimens 12-S- 1 and 12-K- 2, for example, it can be seen that the values for 'max' and 'crack' are identical. However, it can also be seen that there are only small differences ($\leq$ 5%) for specimens 12-S- 6, 12-K- 4, and 12-K- 10, while there is a greater difference (> 5%) for other specimens such as 12-S- 2 and 12-K- 7.

The differences can be attributed to the high number of individual competing notches (pitting vs. welds and combination of both) on the specimen's surface. Consequently, factors other than the notch sharpness determine the exact crack initiation locations. An example is the variation in material properties on the specimen's surface or the difference between the base and weld material. This can lead to deviations between the crack locations observed in fatigue tests and those predicted numerically. Additionally, the determination of effective notch stress concentration from numerical analysis may be inaccurate due to the selected meshing methodology, which is not uniformly defined over the whole corroded area. Furthermore, particularly for butt-welded specimens, the mismatch can be caused by additional bending stresses from the clamping process. Although the clamping process was simulated, the changes in the mean stress resulting from it were not considered. Moreover, the residual stresses and their distribution over the entire specimen may influence the exact crack location but were not known in this study.

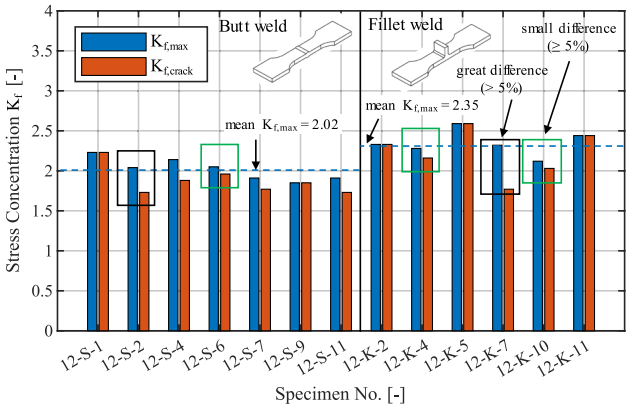

Fig. 13 Effective notch stress concentrations K_f resulting from numerical analysis

In view of these challenges in the modelling, a difference in the effective notch stress concentrations between 'max' and 'crack' of approx. 5% (small difference) is classified as a match. This means a match for a total of 8 out of 13 specimens or 62%. The welded corroded specimens from Shojai et al. [16], which were only exposed to corrosion for 1 month, had a much higher agreement, with 90% for butt welds and 100% for fillet welds, than the 12-month corroded specimens in this study. Potential reasons for this behaviour are discussed in the following section.

In Fig. 14 (a), all fatigue test results are illustrated in one S–N diagram based on the nominal stresses $\Delta\sigma_n$, showing a scatter of $T_\sigma = 1.78$. In Fig. 14 (b), all fatigue test data are plotted based on the effective notch stresses $\Delta\sigma_f$, indicating a scatter of $T_\sigma = 1.45$. The effective notch stresses were calculated by multiplication of the effective notch stress concentration at the crack location with the nominal stresses: $\Delta\sigma_f = K_{f,crack}\ \Delta\sigma_n$. The evaluation based on the effective notch stresses thus shows a reduction in the scatter. The scatter is very low at high stress ranges, while it is greater at low stress ranges. Despite the reduced scatter, there is a clear difference between the uncorroded and corroded specimens. This difference is attributed to the fact that the material near the surface of the corroded specimens is brittle compared to the uncorroded specimens. This can be taken into account in the numerical calculation via a reduced weighting parameter a, but was not done in this study for the purpose of comparability. Furthermore, it can be observed that the originally narrow scatter within the 12 M specimens (see Fig. 14 (a)) has, contrary to expectations, become higher by taking the notch stresses into account (see Fig. 14 (b)). Potential reasons are discussed in the following section.

3.3 Discussion

The results of the fatigue tests have shown that a corrosion duration of 12 months in the SSC significantly influences the fatigue strength. It was found that the fatigue strength decreases for all specimen geometries compared to the uncorroded state, but the decrease varies depending on the specimen geometry. The investigations showed that corrosion may have an equalization effect, which leads all specimens to have similar fatigue strengths after

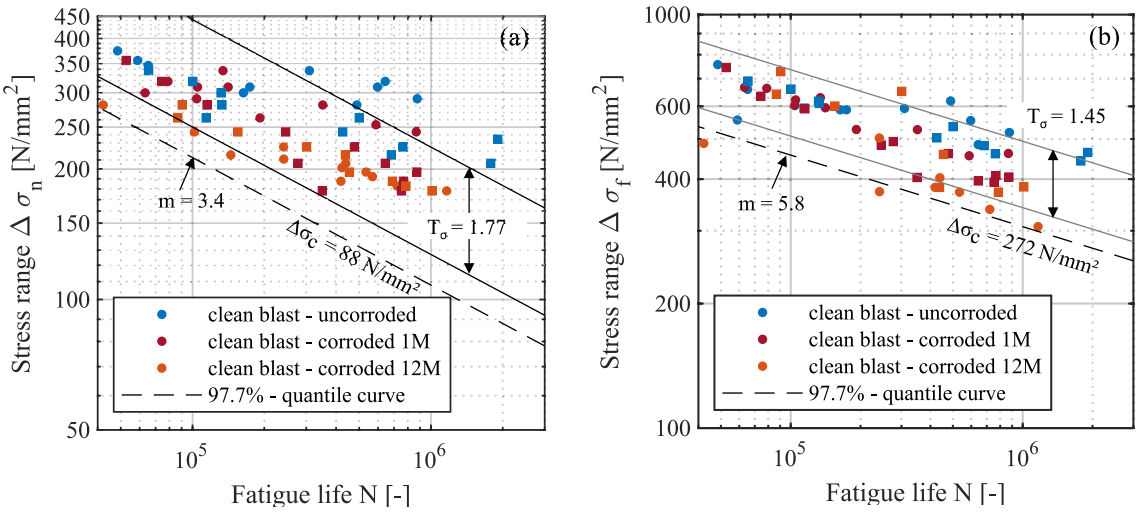

Fig. 14 Evaluation of all fatigue test data based on **a** nominal stresses and **b** effective notch stresses from numerical analysis

a certain exposure duration. For butt and fillet welds, it was observed that after 12 months there was almost no difference in fatigue strength, although they showed significant differences in the uncorroded state. A similar pattern was observed in the study of Yuasa and Watanabe [11], where pre-corroded fillet- and butt-welded specimens were tested on fatigue. It was found that the fatigue strength of butt-welded joints decreased, while it remained unchanged for fillet-welded joints. This is because the already very sharp notches of the fillet welds could not be further intensified by corrosion, whereas the stress concentration of the butt welds had more potential to increase due to their initially low notch sharpness. This is in line with the observations in [5, 36], where the initial notch sharpness of butt welds increased due to corrosion, while it decreased for fillet welds.

The numerical analysis revealed that the exact crack location could only be predicted for approximately 62% of all specimens. This can partly be attributed to inaccuracies arising from the reverse engineering process, including scanning, as well as from the numerical simulations, particularly the selected meshing methodology. Additionally, this can be due to the high number of competing notches in these specimens, such as welds, pitting, or their interactions. In such cases, other factors, like local material behaviour or residual stresses in the notch, become significant. In this study, material behaviour was assumed to be uniform across the entire specimen. Residual stresses, on the other hand, were not included in the numerical calculations due to the lack of measurements covering the entire surface.

In contrast to the 12-month corroded specimens, the 1-month corroded specimens [16] showed an agreement of over 90%. This was possible because cracks in all 1-month corroded specimens initiated in the heat-affected zone (HAZ) directly at the weld toe, whereas for the 12-month corroded specimens, cracks occurred both at the HAZ and in the base material. As a result, the 1-month corroded specimens can be assumed to exhibit uniform material behaviour, which is not the case for the 12-month corroded specimens. Furthermore, since the cracks in the 1-month corroded specimens always initiated in the HAZ, a single-point residual stress measurement at the HAZ was sufficient.

Consequently, for a higher prediction rate of the crack location, the residual stress distribution over the entire specimen must be examined and superimposed with the effective notch stress distribution. In addition, consideration of the different material behaviour of the HAZ and the base material could further improve the agreement rate.

Despite the low agreement rate of crack locations, considering the notch stress concentrations made it possible to reduce the scatter in the combined S–N curve, which includes both butt and fillet weld specimens, as well as specimens with varying corrosion durations. The derived S–N curve, with $\Delta\sigma_c = 272$ N/mm^2 and $m = 5.8$, can be interpreted as a master S–N curve. In the future, this curve could be used to investigate the fatigue strength of corroded specimens using the notch stress approach.

Similar to the notch stress S–N curve FAT 225 according to IIW, which is valid only with an averaging length of 0.4 mm, the master curve derived here is only applicable with a parameter $a = 0.01$ mm^2. Additionally, it is important to note that this master curve is only valid for clean-blasted components, as the specimens used to derive it were also clean blasted. The clean-blasting process can also explain why the S–N curve derived here

is higher compared to FAT 225. This is because FAT 225 is primarily calibrated for as-welded specimens, which exhibit high tensile residual stresses at the weld seam. In contrast, clean-blasted specimens primarily have compressive residual stresses, which remain largely unchanged during the corrosion process [36].

4 Summary and conclusion

The aim of this study was to investigate the long-term influence of corrosion on fatigue strength. The focus was primarily on the change in the notch effect due to corrosion and the associated change in fatigue strength. For this purpose, both base material (11 specimens) and welded joints such as butt welds (13 specimens) and fillet welds (9 specimens) were clean blasted according to offshore requirements and subsequently pre-corroded in a SSC for 12 months. Before the fatigue tests, the specimens were 3D scanned and transformed into numerical models using reverse-engineering methods. The numerical models were used to determine the effective notch stress concentrations based on the real geometry and compared with the crack locations from the fatigue tests.

The following conclusions can be drawn from this investigation:

- After 12 months of exposure, the characteristic fatigue strength of the base material specimens was reduced from $\Delta\sigma_c = 282$ N/mm^2 in the uncorroded state to $\Delta\sigma_c = 122$ N/mm^2. The butt-welded specimens showed a reduction from $\Delta\sigma_c = 215$ N/mm^2 to $\Delta\sigma_c = 147$ N/mm^2. The fillet weld specimens showed the lowest reduction from $\Delta\sigma_c = 168$ N/mm^2 to $\Delta\sigma_c = 144$ N/mm^2. From this, it can be concluded that the fatigue strength reduction depends on the initial fatigue strength and is not the same for different specimen geometries.
- The impact of corrosion on the fatigue strength reduction is greater for not or moderately pre-notched components, such as base material or butt welds, than for strongly pre-notched components, such as fillet welds.
- The fatigue tests indicate an equalizing effect over a long exposure period. Regardless of the initial state, the fatigue strength after 12 months of corrosion is very similar for all specimen geometries. Corrosion causes weak notches to become sharper and sharp notches to become smoother, causing the fatigue strength of different pre-notched specimens to be equalized. Thus, the joint evaluation of all specimen geometries led to a fatigue strength of $\Delta\sigma_c = 133$ N/mm^2 with a narrow scatter of $T_\sigma = 1.33$.
- The numerical investigation showed that in 8 out of 13 cases, the crack location from the fatigue test could be predicted. In these cases, the location of the highest effective notch stress concentration matched the actual crack location. The effective notch stress concentrations, as a result of pitting corrosion and welds, are thus assumed to have a high impact on the fatigue strength.
- The numerical prediction rate of the crack location is lower for the 12-month corroded specimens compared to investigations on welded specimens that have been corroded for 1 month. This is attributed to the greater number of competing notches (pitting vs. welds), the different residual stresses at the weld seam and in the area of the base material, as well as the different material behaviour in the HAZ and base material.

The results of the fatigue tests can be used to better assess the remaining service life of existing corroded components. In addition, the numerical investigation contributes to quantifying the remaining service life on the basis of 3D digital scans and thus enables deployments of digital twins and predictions to be made on the basis of the existing condition of the structures. For this purpose, however, further investigations, including detailed information on the residual stress distribution under consideration of the different material behaviour within the specimens, will be necessary in the future.

Appendix 1. Fatigue test results

Fatigue test results for all specimens.

Table 4 Results of the fatigue tests after 12 months of corrosion exposure in the salt spray chamber

Specimen no	Max. load F_{max} (kN)	Min. load F_{min} (kN)	Cross section (mm^2)	Stress range $\Delta\sigma$ (N/mm^2)	Cycles N (-)	Comments
12-G- 01	170	17	480	318.7	32,335	
12-G- 02	150	15	480	281.2	76,624	
12-G- 03	87.5	8.75	480	164.0	663,635	
12-G- 04	100	10	480	187.5	562,082	
12-G- 05	130	13	480	243.7	177,270	
12-G- 06	87.5	8.75	480	164.0	1,042,404	
12-G- 07	87.5	8.75	480	164.0	1,041,486	
12-G- 08_1	80	8	480	150	2,000,000	Run-out
12-G- 08_2	105	10.5	480	196.8	558,375	Run-out, tested on new load level
12-G- 10	90	9	480	168.7	522,284	
12-G- 11_1	85	8.5	480	159.3	2,000,000	Run-out
12-G- 11_2	130	13	480	243.7	113,235	Run-out, tested on new load level
12-G- 12_1	86.5	8.65	480	162.1	2,000,000	Run-out
12-G- 12_2	140	14	480	262.5	59,872	Run-out, tested on new load level
12-S- 01	120	12	480	225	241,008	
12-S- 02_1	90	9	480	168.7	2,000,000	Run-out
12-S- 02_2	150	15	480	281.2	42,189	Run-out, tested on new load level
12-S- 03	115	11.5	480	215.6	144,678	
12-S- 04	105	10.5	480	196.8	533,996	
12-S- 05	100	10	480	187.5	419,075	
12-S- 06	110	11	480	206.2	439,263	
12-S- 07	112.5	11.25	480	210.9	241,382	
12-S- 08	107.5	10.75	480	201.5	423,550	
12-S- 09	97.5	9.75	480	182.8	721,179	
12-S- 10	100	10	480	187.5	767,154	
12-S- 11	95	9.5	480	178.1	1,163,928	
12-S- 12	130	13	480	243.7	101,845	
12-S- 13	102.5	10.25	480	192.1	568,341	
12-K- 01	100	10	480	187.5	689,101	
12-K- 02	105	10.5	480	196.8	455,001	
12-K- 04	95	9.5	480	178.1	1,010,584	
12-K- 05	150	15	480	281.2	90,576	
12-K- 06	120	12	480	225	300,761	
12-K- 07	115	11.5	480	215.6	437,867	
12-K- 09	130	13	480	243.7	154,975	
12-K- 10	97.5	9.75	480	182.8	785,485	
12-K- 11	140	14	480	262.5	86,751	

Appendix 2. Numerical analysis results

Effective notch stress concentrations from numerical analysis and comparison with cracks from fatigue tests for all analysed specimens.

Butt-welded specimens:

Specimen No. 12-S-1

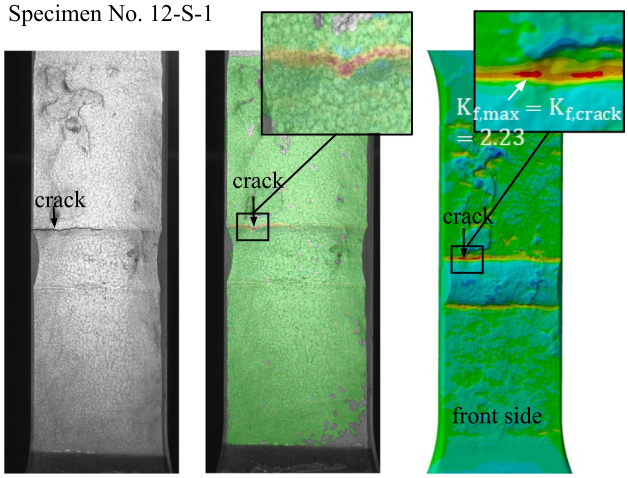

DIC-shot DIC-strain Effective notch stress concentration

Specimen No. 12-S-2

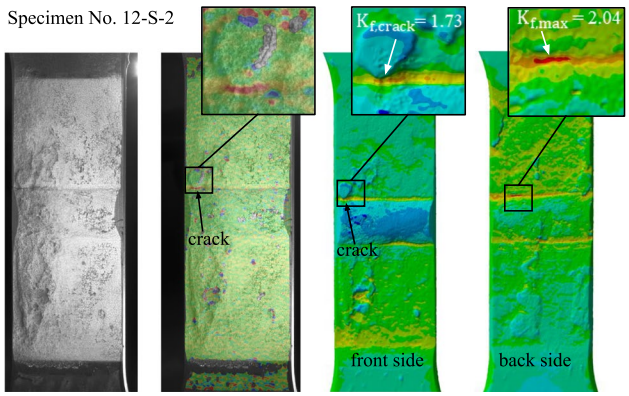

DIC-shot DIC-strain Effective notch stress concentration

Specimen No. 12-S-4

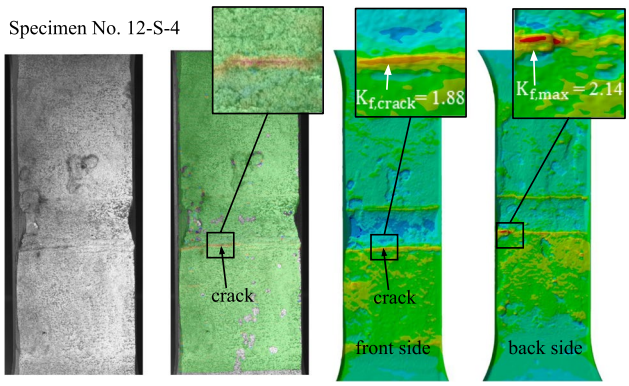

DIC-shot DIC-strain Effective notch stress concentration

Specimen No. 12-S-6

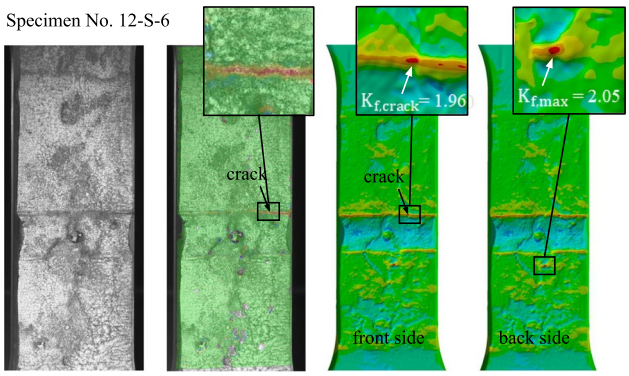

DIC-shot DIC-strain Effective notch stress concentration

Specimen No. 12-S-7

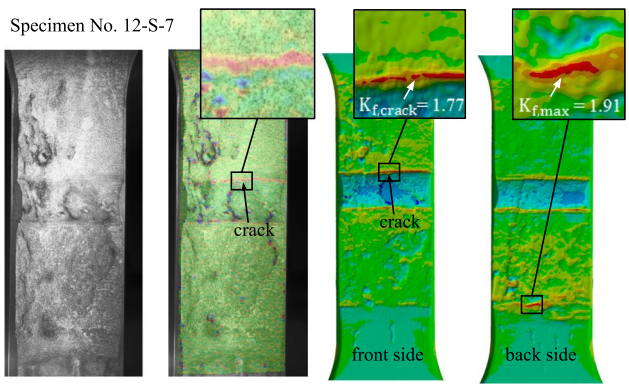

DIC-shot DIC-strain Effective notch stress concentration

Specimen No. 12-S-9

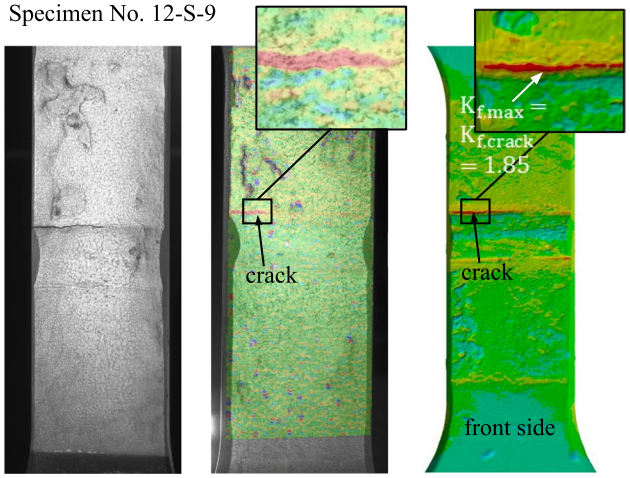

DIC-shot DIC-strain Effective notch stress concentration

Specimen No. 12-S-11

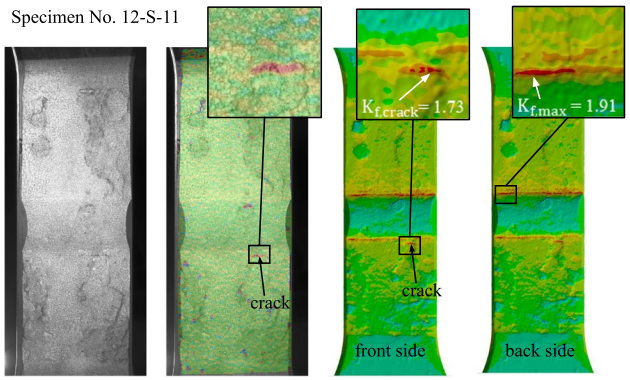

DIC-shot DIC-strain Effective notch stress concentration

Fillet-welded specimens:

Specimen No. 12-K-2

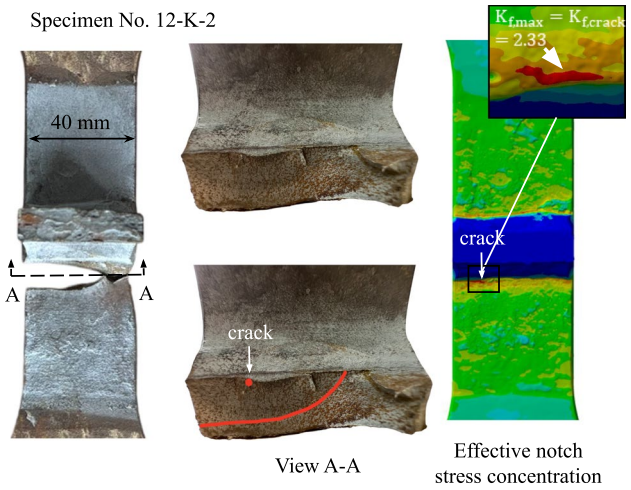

View A-A Effective notch stress concentration

Specimen No. 12-K-4

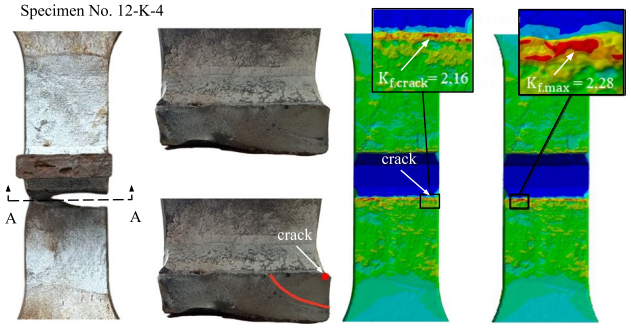

View A-A Effective notch stress concentration

Specimen No. 12-K-5

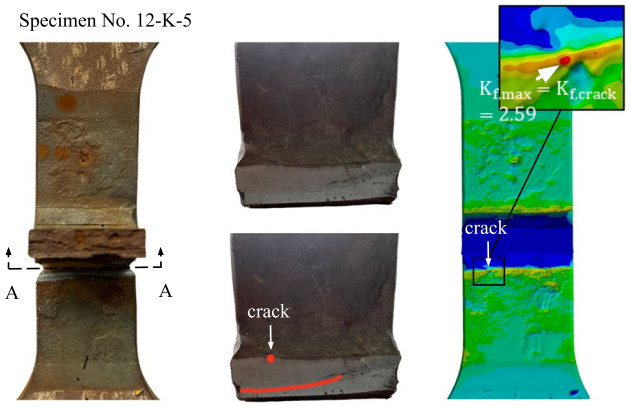

View A-A Effective notch stress concentration

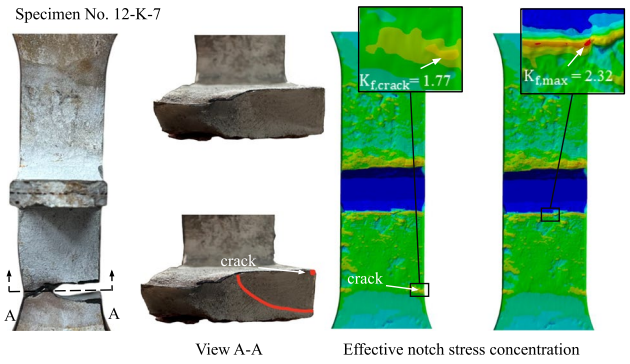

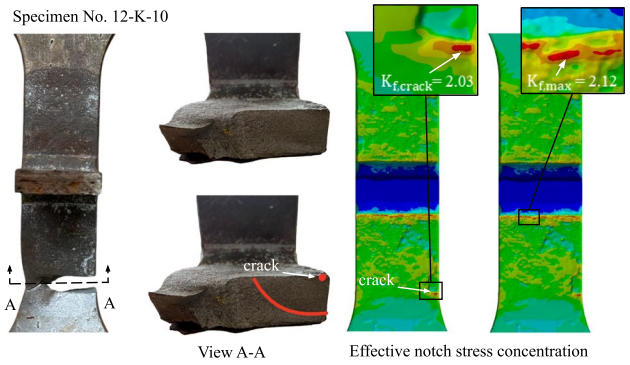

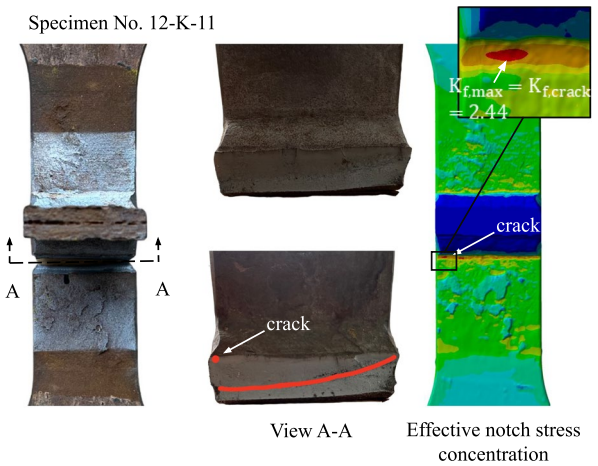

Author contribution Sulaiman Shojai: conceptualization, methodology, validation, formal analysis, investigation, writing — original draft, writing — review and editing, visualization, project administration, funding acquisition.

Kram Kabha: conceptualization, methodology, validation, formal analysis, investigation, writing — review and editing, visualization.

Christian Woitzik: resources, writing — review and editing.

Moritz Braun: writing — review and editing, funding acquisition.

Elyas Ghafoori: writing — review and editing.

Funding Open Access funding enabled and organized by Projekt DEAL. The authors express their sincere gratitude for the financial support of the research project 'Influence of corrosive media on the fatigue strength of offshore wind turbines (CorroFAT)', grant number 37 LN/1, of the Research Association for Steel Applications (FOSTA) e. V., funded by the German Federal Ministry of Economics and Climate Action (BMWK) via the German Federation of Industrial Research Associations 'Otto von Guericke' (AiF) e. V. on the basis of a resolution of the German Bundestag.

Data availability The data generated and analysed during the current study are available from the corresponding author upon reasonable request.

Declarations

Conflict of interest The authors declare no competing interests.

References

1. Xu S, Qiu B (2013) Experimental study on fatigue behavior of corroded steel. Mater Sci Eng, A 584:163–169. https://doi.org/10.1016/j.msea.2013.07.006
2. Shojai S, Schaumann P, Braun M, Ehlers S (2022) Influence of pitting corrosion on the fatigue strength of offshore steel structures based on 3D surface scans. Int J Fatigue 164:107128. https://doi.org/10.1016/j.ijfatigue.2022.107128
3. Xu S, Wang Y (2015) Estimating the effects of corrosion pits on the fatigue life of steel plate based on the 3D profile. Int J Fatigue 72:27–41. https://doi.org/10.1016/j.ijfatigue.2014.11.003
4. Qvale P, Zarandi EP, Ås SK, Skallerud BH (2021) Digital image correlation for continuous mapping of fatigue crack initiation sites on corroded surface from offshore mooring chain. Int J Fatigue 151:106350. https://doi.org/10.1016/j.ijfatigue.2021.106350
5. Shojai S, Brömer T, Ghafoori E, Woitzik C, Braun M, Köhler M et al (2023) Assessment of corrosion fatigue in welded joints using 3D surface scans, digital image correlation, hardness measurements, and residual stress analysis. Int J Fatigue 176:107866. https://doi.org/10.1016/j.ijfatigue.2023.107866
6. Gkatzogiannis S, Weinert J, Engelhardt I, Knoedel P, Ummenhofer T (2021) Corrosion fatigue behaviour of HFMI-treated butt welds. Int J Fatigue 145:106079. https://doi.org/10.1016/j.ijfatigue.2020.106079
7. Gkatzogiannis S, Weinert J, Engelhardt I, Knoedel P, Ummenhofer T (2019) Correlation of laboratory and real marine corrosion for the investigation of corrosion fatigue behaviour of steel components. Int J Fatigue 126:90–102. https://doi.org/10.1016/j.ijfatigue.2019.04.041

8. Det Norske Veritas - Germanischer Llyod. Fatigue design of offshore steel structures (DNV-GL RP-C203); 2019.
9. Hobbacher AF (2016) Recommendations for fatigue design of welded joints and components. Springer International Publishing, Cham
10. Health & Safety Executive. Background to new fatigue guidance for steel joints and connections in offshore structures(OTH 92 390); 1998.
11. Yuasa M, Watanabe T (1996) Fatigue strength of corroded weld joints. ClassNK Technical Bull 14:51–61
12. International Standards Organization. ISO 5817: welding – fusion-welded joints in steel, nickel, titanium and their alloys (beam welding excluded) – quality levels for imperfections; 2014.
13. Det Norske Veritas. Corrosion protection for wind turbines (DNV-GL RP-0416); 2016.
14. International Standards Organization (2017) ISO 9227: corrosion tests in artificial atmospheres – salt spray tests. Beuth, Berlin
15. ISO 8407 (2021) corrosion of metals and alloys – removal of corrosion products from corrosion test specimens. Berlin: Beuth
16. Shojai S, Brömer T, Ghafoori E, Schaumann P (2023) Application of local fatigue approaches on corroded welded joints with consideration of weld geometry and residual stresses. Theoretical Appl Fracture Mechanics 129:104215. https://doi.org/10.1016/j.tafmec.2023.104215
17. Shojai S, Schaumann P, Brömer T (2022) Probabilistic modelling of pitting corrosion and its impact on stress concentrations in steel structures in the offshore wind energy. Mar Struct 84:103232. https://doi.org/10.1016/j.marstruc.2022.103232
18. Neuber H (1958) Kerbspannungslehre: Grundlagen für genaue Festigkeitsberechnung mit Berücksichtigung von Konstruktionsform und Werkstoff. Berlin, Heidelberg, s.l.: Springer Berlin Heidelberg; https://doi.org/10.1007/978-3-642-53069-2.
19. Radaj D, Vormwald M (2007) Ermüdungsfestigkeit: Grundlagen für Ingenieure, 3rd edn. Springer-Verlag, Berlin Heidelberg, Berlin, Heidelberg
20. Lazzarin P, Berto F (2005) Some expressions for the strain energy in a finite volume surrounding the root of blunt V-notches. Int J Fract 135(1–4):161–185. https://doi.org/10.1007/s10704-005-3943-6
21. Berto F, Lazzarin P (2009) A review of the volume-based strain energy density approach applied to V-notches and welded structures. Theoret Appl Fract Mech 52(3):183–194. https://doi.org/10.1016/j.tafmec.2009.10.001
22. Song W, Liu X, Berto F, Wang P, Fang H (2017) Fatigue failure transition analysis in load-carrying cruciform welded joints based on strain energy density approach. Fat Frac Eng Mat Struct 40(7):1164–1177. https://doi.org/10.1111/ffe.12588
23. Taylor D (2008) The theory of critical distances. Eng Fract Mech 75(7):1696–1705. https://doi.org/10.1016/j.engfracmech.2007.04.007
24. Susmel L (2008) The theory of critical distances: a review of its applications in fatigue. Eng Fract Mech 75(7):1706–1724. https://doi.org/10.1016/j.engfracmech.2006.12.004
25. Susmel L, Taylor D (2011) The theory of critical distances to estimate lifetime of notched components subjected to variable amplitude uniaxial fatigue loading. Int J Fatigue 33(7):900–911. https://doi.org/10.1016/j.ijfatigue.2011.01.012
26. Peerlings RH, Borst R de, Brekelmans WAM, Vree JHP de (1995) Computational modelling of gradient-enhanced damage for fracture and fatigue problems. In: Owen DRJ, Oñate E, editors. Computational plasticity: fundamentals and applications ; proceedings of the fourth international conference held in Barcelona, Spain, 3th - 6th April, 1995 ; [a book in memoriam of Juan Carlos Simo. Swansea: Pineridge Press p. 975–986.
27. Peerlings RHJ, Brekelmans WAM, de Borst R, Geers MGD (2000) Gradient-enhanced damage modelling of high-cycle fatigue. Int J Numer Meth Engng 49(12):1547–1569
28. Askes H, Livieri P, Susmel L, Taylor D, Tovo R (2013) Intrinsic material length, theory of critical distances and gradient mechanics: analogies and differences in processing linear-elastic crack tip stress fields. Fatigue Fract Engng Mater Struct 36(1):39–55. https://doi.org/10.1111/j.1460-2695.2012.01687.x
29. Tovo R, Livieri P, Benvenuti E (2006) An implicit gradient type of static failure criterion for mixed-mode loading. Int J Fract 141(3–4):497–511. https://doi.org/10.1007/s10704-006-9011-z
30. de Borst R, Pamin J, Peerlings RHJ, Sluys LJ (1995) On gradient-enhanced damage and plasticity models for failure in quasi-brittle and frictional materials. Comput Mech 17(1–2):130–141. https://doi.org/10.1007/s004660050098
31. Lener G, Lang R, Ladinek M, Timmers R (2018) A numerical method for determining the fatigue strength of welded joints with a significant improvement in accuracy. Procedia Eng 213:359–373. https://doi.org/10.1016/j.proeng.2018.02.036
32. Lang R, Ladinek M, Lener G (2017) Über die Anpassung eines fortschrittlichen Stützwirkungsansatzes für das Kerbspannungskonzept. Stahlbau 86(6):470–482. https://doi.org/10.1002/stab.201710494
33. Shojai S, Schaumann P, Ghafoori E (2024) Micro-support effect consideration in fatigue analysis of corroded steel based on real surface geometry. J Constr Steel Res 212:108259. https://doi.org/10.1016/j.jcsr.2023.108259
34. Tovo R, Livieri P (2007) An implicit gradient application to fatigue of sharp notches and weldments. Eng Fract Mech 74(4):515–526. https://doi.org/10.1016/j.engfracmech.2006.06.009
35. European Committee for Standardization. Eurocode 3 - Design of steel structures - Part 1–9: Fatigue(EN 1993–1–9); 2020.
36. Shojai S, Schönamsgruber F, Köhler M, Ghafoori E (2025) Impact of accelerated corrosion on weld geometry, hardness and residual stresses of offshore steel joints over time. Materials Design 251:113578. https://doi.org/10.1016/j.matdes.2024.113578